JOURNAL OF GEOPHYSICAL RESEARCH, VOL. 100, NO. C9, PAGES 18,597–18,609, SEPTEMBER 15, 1995

Runout and fine-sediment deposits of axisymmetric turbidity currents

W. Brian Dade and Herbert E. Huppert

Institute of Theoretical Geophysics, Department of Earth Sciences and Department of Applied Mathematics and Theoretical Physics, University of Cambridge, Cambridge, England

ABSTRACT. We develop a model that describes the runout behavior and resulting deposit of a radially spreading, suspension-driven gravity current on a surface of negligible slope. Our analysis considers the separate cases of constant-volume and constant-flux sources. It incorporates expressions for the conservation of volume, a Froude number condition at the current front, and the evolution of the driving suspension due to settling of particles to the underlying bed. The model captures the key features of a range of experimental observations. The analysis also provides important scaling relationships between the geometry of a deposit and the source conditions for the deposit-forming flow, as well as explicit expressions for flow speed and deposit thickness as functions of radial distance from the source. Among the results of our study we find that, in the absence of information regarding flow history, the geometries of relatively well-sorted deposits generated by flows with source conditions of constant volume or constant flux are virtually indistinguishable. The results of our analysis can be used by geologists in the interpretation of some geologically important gravity-surge deposits. Using our analytical results, we consider three previously studied, radially symmetric turbidites of the Hispaniola-Caicos basin in the western Atlantic Ocean. From gross geometry and grain size of the turbidites alone we estimate for the respective deposit-forming events that upon entry into the basin the initial sediment concentrations were approximately 3% by volume and the total volumes were roughly between 30 km^3 and 100 km^3. Each of the suspension-driven flows is inferred to have spread into the basin with a characteristic speed of 3–5 m s^{-1}, and reached its ultimate runout length of about 60–75 km while laying down a deposit over a period of about 10–12 hours.

Introduction

A gravity current results from a difference in density between two fluids. Geologically important gravity currents include turbidity currents which occur as relatively dense underflows in the ocean and in lakes. Turbidity currents derive their excess density from fine particles which are maintained in suspension by turbulence generated by the mean flow. Deposition by turbidity currents occurs primarily on surfaces of negligible slope.

In this paper we present an approximate model for the propagation of and the deposition from a suspension-driven gravity current spreading radially into a relatively flat basin. In one application of the model we consider the flow that results from the instantaneous release of a dense suspension with a finite volume. A second application pertains to the case in which the flow is maintained under conditions of constant flux. The approach we take here represents an extension of the model developed by *Huppert and Simpson* [1980] for a saline gravity current in which buoyancy is conserved. Elsewhere we have successfully modified the Huppert and Simpson model to include the effects of buoyancy loss through sediment deposition in the case of a channelized, constant-volume flow [*Dade and Huppert*, 1994, 1995]. Similarly, we have elsewhere developed a theory for a channelized, deposit-forming gravity surge propagating down slope and for which the entrainment of ambient fluid is important [*Dade et al.*, 1994]. Here, however, we consider the behavior of a nonchannelized, radially spreading flow which is progressively diluted owing to sediment deposition. The results of our analysis are found to agree well with observations of deposit-forming gravity currents generated in the laboratory. A more complete but wholly numerical treatment of the fluid mechanics of these phenomena is given by *Bonnecaze et al.* [1993; 1995].

In the following section we present an analysis of the equations that describe the behavior of a gravity current which results from the release of a particle suspension with finite volume. Our analysis provides explicit expressions for the position of the current front as a function of time and the distribution of particle deposit as a function of radial distance from the point of release. We pursue a similar consideration for the behavior of a flow in which the overall volume flux is held constant. The results of these analyses are shown to compare well with experimental observations. We then introduce an additional level of complexity by discussing briefly the effects of buoyancy reversal on the runout length of a gravity current. Finally, we discuss our analytical results in the context of some previously studied turbidites of the Hispaniola-Caicos basin of the western Atlantic Ocean.

Paper number 95JC01917.
0148-0227/95/95JC-01917$05.00

Gravity Currents With Constant Volume

Governing Equations

We begin by considering a well-mixed, suspension-driven gravity current released from a lock and spreading radially over a rigid, horizontal surface. A key assumption of this

model is that the axisymmetric gravity current is instantaneously well mixed in both the vertical and radial directions and evolves en masse as the flow propagates outward. The flow is thus considered to be an axisymmetrically spreading cylinder which has uniform properties at any instant in time. The total volume of particles is assumed to be a small fraction of the total volume of the flow. Additionally, we assume that entrainment of ambient fluid is negligible and so the volume of the current is conserved [cf. *Hallworth et al.*, 1993]. At any instant in time the geometry of this radially-spreading flow requires that

$$q_0' = \Theta \pi r^2 h, \tag{1}$$

where q_0' is the initial volume of the flow, r is the radial distance from the origin to the advancing front, and h is the radially averaged thickness of the spreading current. The prefactor $\Theta = \theta/2\pi$ is the normalized angle θ of the sector through which the current is propagating; Θ is unity for a current spreading uniformly in all directions and 0.5 for a current debouching into a basin from a side entry point. We continue our analysis for the augmented volume $q_0 = \Theta^{-1} q_0'$ and assume that the current spreads uniformly in all directions. This prefactor will be reintroduced, however, in a consideration of experimental flows and in the reconstruction of the gravity currents which resulted in the turbidites of the Hispaniola-Caicos basin.

Returning to our model, we consider a gravity current to be driven by particles that have density ρ_p and which are present in volumetric concentration ϕ. The particles are suspended in an interstitial fluid of density ρ_i and the suspension-driven flow is spreading into an ambient fluid of density ρ_a. For an inertial flow the rate of radial advance of the current front is related to the driving buoyancy through the Froude number Fr at the front of the current by

$$\frac{dr}{dt} = u = Fr\left[g_p'\left(\phi - \phi_{cr}\right)h\right]^{1/2}, \tag{2}$$

where $r = r_0$ at $t = 0$, $g_p' = g(\rho_p - \rho_i)/\rho_a$, and $\phi_{cr} = (\rho_a - \rho_i)/(\rho_p - \rho_i)$. The product $g_p'(\phi - \phi_{cr}) = g'$ is the reduced gravity of the bulk flow and quantifies the density difference that drives the current. The parameter ϕ_{cr} is the critical ratio of the density difference between the ambient and interstitial fluids to that between the particles and interstitial fluid. When ambient and interstitial fluids have the same density, $\phi_{cr} = 0$. If a gravity current with light interstitial fluid propagates below a denser ambient fluid, however, ρ_a is greater than ρ_i and $\phi_{cr} > 0$. As ϕ diminishes with sedimentation to ϕ_{cr}, the flow becomes neutrally buoyant and is no longer a density-driven undercurrent. Further loss of driving buoyancy will result in the "lift off" of the current from the bed. We will return to this scenario later in the paper.

On the length scale of the head the current can be viewed as being locally two-dimensional and so the Froude number at the head of the flow is found experimentally to be given by

$$Fr = 1/2(h/d)^{-1/3} \qquad h/d > 0.075, \tag{3a}$$

$$Fr = 1.19 \qquad h/d \le 0.075, \tag{3b}$$

where d is the depth of the ambient fluid [*Huppert and Simpson*, 1980]. The depth dependence of Fr in (3a) accommodates the effects of a return flow in the shallow layer of ambient fluid overlying the gravity current. This correction is required for an accurate description of many laboratory flows. When the surrounding fluid becomes very deep relative to the thickness of the gravity current, Fr is constant and close to the value $Fr = \sqrt{2}$ predicted for a perfect, inviscid fluid [*Benjamin*, 1968]. The difference is due to the momentum loss caused by turbulent stresses within the head of the current.

The equation that describes the evolution of particle mass in the well-mixed suspension which drives the flow is given by

$$\frac{db}{dt} = -\frac{w_s b}{h} + F_0, \tag{4}$$

where $b = q\phi$, with the initial condition $b_0 = q_0\phi_0$, and w_s is the average settling speed of the particles in the suspension. The first term on the right-hand side of (4) reflects the arrival rate $w_s\phi$ of material settling from the suspension over an area of the bed q_0/h overlain by the current at any instant in time. Similarly, the term F_0 represents the total vertical turbulent flux of sediment at the bed over the same area and quantifies the capacity of the flow to maintain sediment in suspension or the competence of the flow to rework newly deposited sediment.

Applicability of (4) requires that the driving suspension be well mixed. That is, the ratio of particle settling speed w_s to average flow speed u is much less than unity. We show in Appendix A that the sediment erosion term F_0 in (4) should become negligible within the body of the flow if the ratio w_s/u is greater than $\sin\beta$, where β is the slope of the bed over which the gravity current propagates. This constraint reflects the energetic demands made on the mean flow in the maintenance of both turbulence and a dense sediment suspension. Thus (4) with vanishing F_0 describes the evolution of a fine-sediment suspension under the conditions

$$\sin\beta < w_s/u << 1. \tag{5}$$

In general this constraint also obviates the need to consider entrainment of ambient fluid.

Gravity Currents in Deep Surroundings and $\phi_{cr} = 0$

Consider a flow over a horizontal bed for which $h/d \le 0.075$ and the densities of interstitial and ambient fluids are equal. Division of (4) by (2), subject to constant Fr per (3b) and the constant-volume constraint of (1) yields a differential equation whose solution describes the spatial evolution of the driving buoyancy in the spreading flow. This expression can be recast in terms of the dimensionless volumetric fraction of particles in suspension $\Phi = \phi/\phi_0$, where the subscript 0 denotes initial values and the dimensionless radial distance $R = r/r_\infty$, where r_∞ is the final runout length evaluated below. Both Φ and R are independent variables and take on values between 0 and 1. Solving the equations and carrying out the nondimensionalization, we obtain the expression

$$\Phi = (1 - R^4)^2, \tag{6}$$

where for convenience r_0 is taken to be the origin. The runout length r_∞ is calculated to be

$$r_\infty = \gamma_d (g_0' q_0^3/w_s^2)^{1/8}, \tag{7}$$

with

$$\gamma_d = (64Fr^2/\pi^3)^{1/8}. \tag{8}$$

If $Fr = 1.19$, then $\gamma_d \approx 1.14$ (with $1.1 \le \gamma_d \le 1.2$ if $1 \le Fr \le \sqrt{2}$).

Note that the concentration of the driving suspension vanishes at $R = 1$. Thus flows initiated from an instantaneous release of a constant volume will in our model exhibit a finite runout distance as a consequence of the loss of all dense material from the driving suspension. In reality, an inertial gravity current will overshoot this mark somewhat owing to residual momentum which must be dissipated by friction before the flow will come to a complete halt.

We now substitute (6) into the nondimensional version of (2) (again, subject to constant Fr) and solve the resulting differential equation, with $R = 0$ at $T \equiv t/t_\infty = 0$ (with the timescale t_∞ evaluated explicitly below). This yields the expression

$$\ln[(1+R^2)/(1-R^2)] = 2T, \tag{9}$$

which relates the position of the spreading current front and time. Equation (9) can be rearranged to give

$$R = \tanh^{1/2} T, \tag{10}$$

where

$$t_\infty = {}^1/_2 \pi^{1/2} \gamma_d^2 Fr^{-1} (q_0/g_0' w_s^2)^{1/4} \approx (q_0/g_0' w_s^2)^{1/4} \tag{11}$$

as the appropriate expressions for R and the runout timescale t_∞. We note that $R = 0.87$ at $T = 1$ (or in equivalent dimensional terms $r = 0.87 r_\infty$ at $t = t_\infty$) and $R = 0.98$ at $T = 2$ ($r = 0.98 r_\infty$ at $t = 2t_\infty$). Equations (8) and (9) and all following expressions for $R(T)$ yield estimates for frontal flow speed that become infinite at the origin if r_0 is strictly interpreted to be zero. They are rigorously applicable only for radial distances away from the source.

Currents in Shallow Surroundings and $\phi_{cr} = 0$

Consider now the case in which $h/d > 0.075$ during the entire history of the spreading current. This is the situation in many laboratory experiments. As before, consider the densities of interstitial and ambient fluids to be equal. We again render (2) into a spatial derivative with the same initial conditions as above but which now includes a Froude number condition with depth dependence per (3a). The solution to the resulting differential equation yields an expression for the radial evolution of the driving buoyancy in the spreading flow that is different from that of (6). This is given by

$$\Phi = (1 - R^{10/3})^2, \tag{12}$$

where the shallow-fluid runout length is now given by

$$r_\infty = \gamma_s H^{1/10} (g_0' q_0^{23/9} / w_s^2)^{3/20} \tag{13}$$

with $H = d/q_0^{1/3}$ and $\gamma_s \approx 0.96$. This result is subtly different from that obtained for the case of deep surroundings and incorporates a weak dependence of flow runout on the relationship between ambient depth and current volume. The primary difference occurs during "slumping" of the current from the lock immediately following release.

Substitution of (12) into (2) subject to (3a), rearrangement of the result, and subsequent integration yield a relationship between time and the position of the front of the radially spreading current in the form

$$T = f(R), \tag{14}$$

where $R = 0$ at $T = 0$ and $f(R)$ is given in Appendix B. Again, $T = t/t_\infty$, but now the runout time for flows in shallow surroundings is given by

$$t_\infty = (2\pi^{1/6}) H^{-1/3} (r_\infty^{24} / g_0'^9 q_0^5)^{1/18} \approx 2.25 H^{-1/5} (q_0^7 / g_0'^9 w_s^{12})^{1/30}. \tag{15}$$

The expression $f(R)$ in (14) (and (B1)) cannot be analytically inverted to obtain an explicit function $R(T)$, but an approximate, empirical inversion is

$$R \approx \tanh[1.75T] \tag{16}$$

with R and T defined with respect to the shallow-water values of r_∞ and t_∞ given in (13) and (15).

Distribution of Deposits

We now present expressions that allow the evaluation of the distribution of a particle deposit which results from a radially spreading gravity current. In the case of a radially uniform flow with constant volume, the local accumulation rate of the fine-sediment deposit is given by the change of the suspended-particle mass per unit of bed area, $-(\pi r^2)^{-1} db/dr$. Integration of this local quantity from any point r to r_∞ yields the total mass per unit of area of bed or areal density η of the deposit at r. This value represents the deposit that could have accumulated during passage of the spreading gravity flow from the time it reached r until the time it reached its ultimate runout distance at r_∞. Implicit in this approach are the assumptions that the current is spatially uniform and extends back to the origin. Mathematically, the calculation of the deposit in dimensionless terms is given by

$$D \equiv \eta / \eta_{av} = \int_R^1 -\frac{1}{X^2} \frac{d\Phi}{dX} dX, \tag{17}$$

where X is a variable of integration and η_{av} is the average density of the deposit and corresponds to the deposit density that would be observed if the particle mass were uniformly distributed over the total area ultimately covered by the radially spreading flow. In the case of deep surroundings this average value is given by

$$\eta_{av} = \rho_p q_0 \phi_0 / \Theta \pi r_\infty^2 = (\rho_p \phi_0)/(\pi \gamma_d^2) (q_0 w_s^2 / g_0')^{1/4} \approx 0.25 (\rho_p \phi_0) (q_0 w_s^2 / g_0')^{1/4}. \tag{18}$$

The average deposit thickness is simply $\eta_{av}/(\rho_p \phi_b)$ where $\phi_b \approx 0.5$ is the volume fraction of solids in the bed. Upon substitution of the derivative of (6) into (17) and integration of the result, we obtain a general expression for the geometry of the deposit given by

$$D = {}^8/_3 - 4R^2 + {}^4/_3 R^6, \tag{19a}$$

or, equivalently,

$$D_0 \equiv \eta/\eta_0 = 1 - {}^3/_2 R^2 + {}^1/_2 R^6, \tag{19b}$$

where η_0 is the density of the deposit near the origin.

The analogous expressions for deposits laid down by axisymmetric currents in relatively shallow surroundings are given by

$$D = {}^{25}/_7 - 5R^{4/3} + {}^{10}/_7 R^{14/3}, \tag{20a}$$

$$D_0 = 1 - {}^7/_5 R^{4/3} + {}^2/_5 R^{14/3}, \tag{20b}$$

where the characteristic density of the shallow-fluid deposit is given by

$$\eta_{av} = \rho_p q_0 \phi_0 / \pi r_\infty^2$$
$$= (\rho_p \phi_0)/(\pi \gamma_s^2)\, H^{-1/5}\, (q_0^{\prime 7} w_s^{18}/g_0^{\prime 9})^{1/30} \qquad (21)$$
$$\approx 0.35\, (\rho_p \phi_0)\, H^{-1/5}\, (q_0^{\prime 7} w_s^{18}/g_0^{\prime 9})^{1/30}.$$

This approach to the calculation of deposit geometry reflects, as has been stated, the notion of a radially uniform flow which extends back to the origin. Development of strong shocks or horizontal gradients near the origin [cf. *Bonnecaze et al.*, 1993; 1995] will render the calculations invalid in that region. We find that (19) and (20) nevertheless capture the essence of the far-field runout geometry of surge deposits and provide basic functional forms which can be compared with observations or more complicated numerical calculations.

Gravity Currents With Constant Flux

Governing Equations

We now consider a quasi-steady gravity current in which the volume flux q is uniform and maintained at the source. These flows are sometimes called "starting plumes" [*Simpson*, 1987]. Entrainment of fluid and sediment is assumed to be negligible, and $\phi_{cr} = 0$ as before. The assumption that flux is constant through any radial surface at a distance r from the origin requires that

$$\dot{q} = 2\pi r h u, \qquad (22)$$

where, as before, h is the thickness and u is the speed of an inertial flow subject to the Froude number constraint of (2). The flux through a sector with angle $2\pi\Theta$ is $\dot{q}' = \Theta \dot{q}$.

At any point in a flow there is a general balance between the local rate of change of sediment concentration, advection, and the gravitational settling of particles. In mathematical terms this balance is given by

$$\frac{\partial \phi}{\partial t} + u \frac{\partial \phi}{\partial r} = -\frac{w_s \phi}{h}, \qquad (23a)$$

or, equivalently, as

$$\frac{1}{u}\frac{\partial \phi}{\partial t} + \frac{\partial \phi}{\partial r} = \pm(2\,\pi\, w_s / \dot{q})\, r\, \phi \qquad (23b)$$

upon rearrangement and substitution of (22). In a relatively slowly varying but fast moving flow the first term on the left-hand side of (23b) is negligible, and the essential balance is one between advection of material from the source and settling. Under these conditions we see that the distribution of particle mass within a gravity current of constant flux is given by

$$\Phi = \exp[-R_f^2], \qquad (24)$$

where as before Φ is the particle concentration normalized by that at $R_f = 0$, but the radial distance is now rendered dimensionless such that $R_f = r/r_f$, where the length scale r_f is given by

$$r_f = (\dot{q}/\pi w_s)^{1/2}. \qquad (25)$$

Unlike the case of a constant-volume gravity current, there is no finite distance over which the mass of particles is completely spent (see (6)) because material is continually introduced at the source for the duration of the flow. Even in the case of a constant-flux source, however, concentration of sediment nevertheless diminishes rapidly with radial distance in excess of the decay or runout length scale r_f.

Substitution of (22), (24) and (25) into (2) subject to a constant Froude number condition yields an expression for the velocity at the front of the flow

$$U_f \equiv \frac{u}{u_f} = \frac{dR_f}{dT_f} = R_f^{-1/3} \exp[-R_f^2/3], \qquad (26)$$

where

$$u_f = \gamma_f (g_0^{\prime 2}\, \dot{q}\, w_s)^{1/6} \qquad (27a)$$

and $T_f = t/t_f$ with

$$t_f = r_f/u_f = 0.56/\gamma_f (\dot{q}/g_0^{\prime} w_s^2)^{1/3}. \qquad (27b)$$

The coefficient γ_f reflects the value of the Froude number for the current front which is understood to be near unity for inertial gravity flows. In fact, $0.72 \le \gamma_f \le 0.93$ for $1 \le Fr \le \sqrt{2}$. We determined γ_f empirically (see below) and found that a reasonable value is given by $\gamma_f \approx 0.85$. This corresponds to $Fr \approx 1.2$, virtually identical to the value for constant-volume flows in deep surroundings (compare (3b)). If the flow is slowly varying, then $U_f(R_f)$ calculated from (26) provides an estimate of the quasi-steady flow speed at a point once the flow front has passed by.

Equation 26 has the analytical solution

$$T_f = -1.04\, i^{2/3} \int_0^{\xi} X^{2/3-1} \exp[-X]\, dX \qquad (28)$$
$$= 1.04\, |\gamma(^2/_3, \xi)|$$

where $i = \sqrt{-1}$ and $|\gamma(a, \xi)|$ denotes the absolute value of the complex Gamma function [*Abramowitz and Stegun*, 1965] evaluated for $a = 2/3$ and where $\xi = -R_f^2/3$. A key aspect of this result is that, unlike the case of currents with constant volume, R_f increases without bound as time proceeds. There is no convenient inversion $R_f(T_f)$ for the full range of dimensionless length and time, but an empirical approximation valid over the interval $0 < T_f < 10$, which should include many practical applications, is given by

$$R_f \approx 2.8 \tanh^{1/2}[0.16 T_f]. \qquad (29)$$

Equation 29 indicates a functional correspondence with the result for constant volume flows (compare (10)).

Distribution of Deposits

At any point in the flow the instantaneous downward volume flux of sediment per unit of bed area is given by $w_s \phi$. An estimate of the local deposit density η for a quasi-steady flow is thus taken as the product of this flux, the particle density, and the time of duration of the flow at that point. Accordingly, the geometry of a deposit generated by a gravity current with constant flux will exhibit the general form

$$D_f \equiv \eta/\eta_0 = \exp(-R_f^2)\, [1 - T_f(R_f)/T_L], \qquad (30a)$$

where η_0 is the deposit density (or thickness) near the origin,

$T_f(R_f)$ is given by (28) and T_L is the dimensionless time of duration of the constant-flux current. Note that (30a) reduces to the expression

$$D_f \approx \exp(-R_f^2) \tag{30b}$$

as T_L becomes large.

Correlation Between Models for Gravity Currents With Constant Volume and Constant Flux

We have already noted a general correspondence between the expressions that describe the rate of advance of constant volume and constant flux currents. We can rationalize this correlation further by noting that in a gravity current of constant volume a characteristic flux is given by $q \approx q_0 t_\infty^{-1}$. Substitution of this scaling into (7) and (11) yields the alternative forms for a deep water surge $r_\infty \approx \gamma_d (q/w_s)^{1/2} \approx 2r_f$ and $t_\infty \approx 0.9 (q/g_0' w_s^2)^{1/3} \approx 0.6 t_f$. The dimensionless equivalents are $2R \approx R_f$ and $0.6T \approx T_f$. The length and timescales over which deposit-forming flows with either constant volume or constant flux relax from otherwise analogous source conditions are thus similar.

Comparison of Theory and Experiment

An extensive experimental program was undertaken by *Bonnecaze et al.* [1995] to provide a test of their numerical calculations for axisymmetric gravity currents. The experiments were performed in radial sector tanks made of clear Perspex, about 2 m in radial extent and of varying radial geometry (Figure 1). Individual suspensions comprised silicon carbide particles ($\rho_p = 3.217$ g cm^{-3}) which were well sorted and had a known diameter in any given flow but ranged in size from 23 μm to 53 μm across all experiments.

Flows With Constant Volume

Individual suspensions were introduced behind a lock and thoroughly mixed before being instantaneously released into an adjoining basin. After the release the position of the current front was recorded as a function of time. After the runout of a current the resulting particle deposit was sampled as a function of radial distance from the lock. In all cases, $\phi_{cr} = 0$. The relevant details of individual experiments are summarized in Table 1.

Representative data for the position of the flow front as a function of time and deposit geometry as a function of radial distance are shown in Figure 2. For a given grain size we see that a more concentrated flow moves farther in less time than does a less concentrated flow (Figure 2a). For a given mass of sediment in the initial suspension, on the other hand, a flow transporting finer-grained sediment will travel farther and thus generate a thinner deposit, on average, than will a flow driven by a suspension of larger particles (Figure 2b).

Comparisons of our theoretical predictions and all experimental observations are presented in Figure 3. The data have been normalized by the analytical scalings r_∞ and t_∞ for shallow surroundings and the observed value of η_0 for each run. We have shown these comparisons on logarithmic axes to emphasize both the early slumping behavior of the laboratory flows in shallow environments [cf. *Huppert and Simpson*, 1980; *Bonnecaze et al.* 1993, 1995; *Dade and Huppert* 1995] and the asymptotic nature of the nondimensional flow and deposit runout at both large times and radial distances.

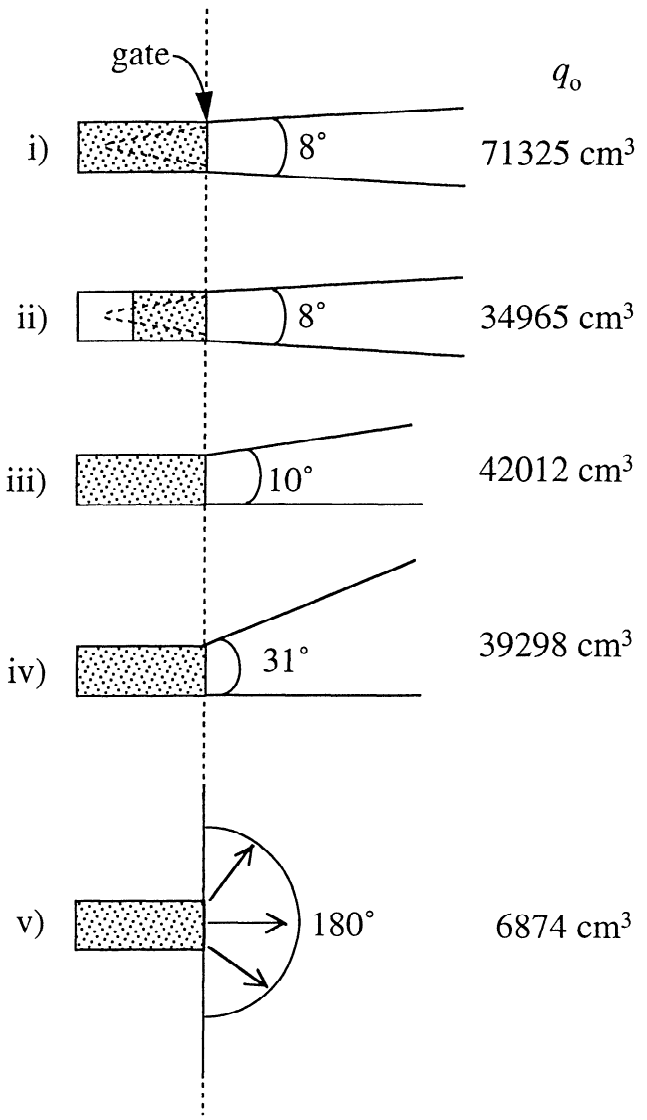

Figure 1. Experimental geometries in plan view used by *Bonnecaze et al.* [1995] in their laboratory study of axisymmetric, suspension-driven gravity currents.

The agreement between theory and experiment is generally good, with the following qualifications. At relatively large times ($T > 1$) a constant-volume flow does not come to rest cleanly, as our simple inertial model would predict, but may rather exhibit weak viscouslike creep beyond the predicted runout distance (Figure 3a). This possibility was noted earlier. Additionally, we note that our model for the distribution of a particle deposit represents a maximal envelope for the geometry of a particle deposit (Figure 3b). This reflects the assumption that a flow extends uniformly back to the origin. Nevertheless, the overall scaling of the runout distance of a flow is well predicted from (13) for the full range of flow conditions examined, as shown in Figure 4. The consistent overprediction of r_∞ revealed in this plot can be accommodated, in part, with a correction for the amount of particle mass deposited behind the lock (Table 1). The small fraction of this material lost from the driving suspension before a flow is released does not contribute to the runout behavior of a gravity current. Additionally, a small reduction in the coefficient 1/2 of (3a), and thus a decrease in the coefficient γ_s of (13), would

Table 1. Details of Experiments for Suspension-Driven Gravity Currents With Constant Volume

Experiment	Diameter, μm	w_s, cm s^{-1}	g_0', cm s^{-2}	r_∞ (Predicted), cm	M_{lock}	M'_{lock}
1	37	0.15	42.7	194.5	0.18	0.06
2	37	0.15	21.3	175.3	0.24	0.09
3	37	0.15	10.7	158.0	0.32	0.14
4	23	0.07	10.7	202.7	0.15	0.04
5	23	0.07	21.3	224.9	0.13	0.04
6	23	0.07	42.7	249.5	0.10	0.03
7	53	0.31	42.7	156.8	0.290	0.10
8	53	0.31	21.3	141.3	0.38	0.15
9	53	0.31	10.7	127.4	0.41	0.13
10	37	0.15	42.6	151.6	0.08	< 0.01
11	37	0.15	21.3	136.6	0.12	< 0.01
12	37	0.15	10.7	123.2	0.16	< 0.01
13	37	0.15	19.1	143.3	0.27	0.14
14	37	0.15	18.5	139.3	0.14	< 0.01
15	37	0.15	19.1	76.0	0.11	0.02

Experiments 1–9 use geometry i, experiments 10–12 use geometry ii, experiment 13 uses geometry iii, experiment 14 uses geometry iv, and experiment 15 uses geometry v (see Figure 1). Variables are defined as follows: w_s, average settling speed of the particles in suspension; g_0', initial reduced gravity; and r_∞, runout length. M_{lock} is the fraction of initial mass of particles deposited behind the lock. M'_{lock} is an estimate of the fraction of total mass in the lock which is in excess of that expected for a near-origin deposit density $\eta_0 = 25/7\ \eta_{av}$ calculated from (21). This quantity thus represents an estimate of the fraction of initial mass which settled out before the release of each constant volume flow and contributed to the observation that r_∞ predicted from (19) overestimates the actual runout distance (see Figure 4).

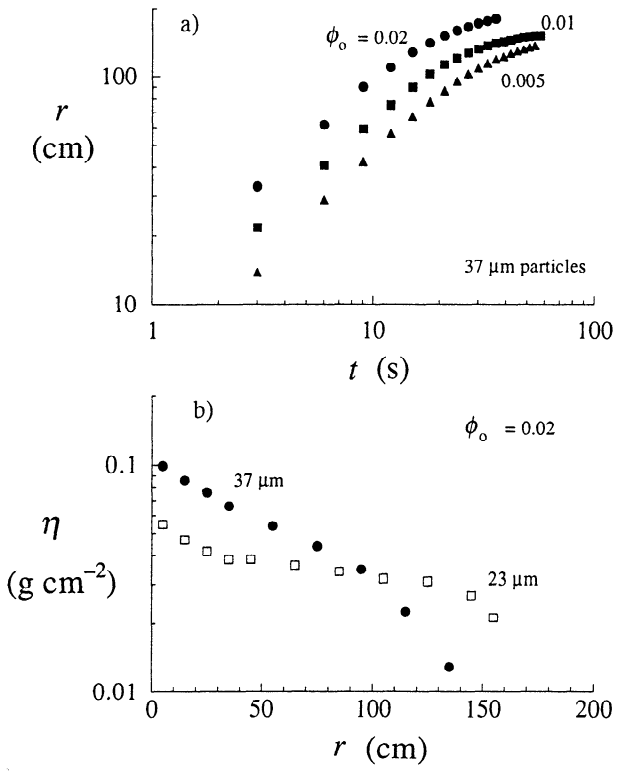

Figure 2. Representative data from the study of *Bonnecaze et al.* [1995] for gravity currents following the instantaneous release of a constant volume of dense suspensions. (a) Position of current front as a function of time since release. The grain size of the particles in the driving suspension was 37 μm, and initial values of the particle concentrations ϕ_0 are indicated. (b) Mass deposited per area of bed as a function of radial distance from the point of release. Initial particle concentration $\phi_0 = 0.02$, and grain sizes of particles are indicated

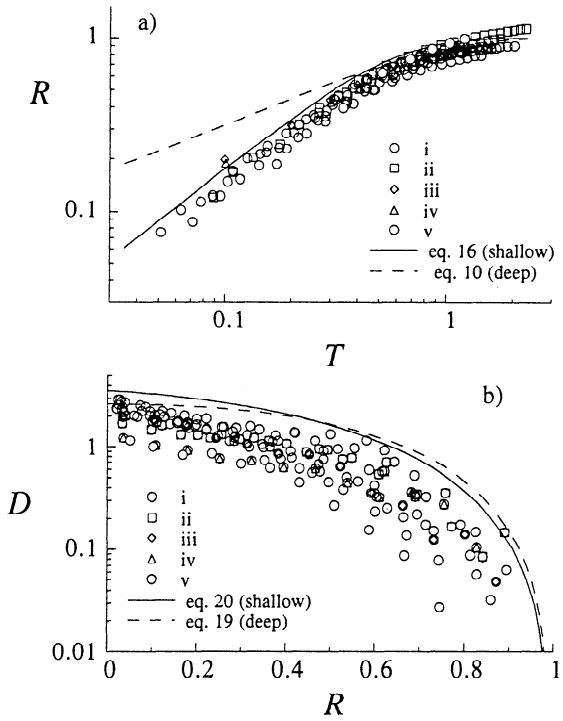

Figure 3. The runout and deposits of axisymmetrically spreading gravity currents following the instantaneous release of dense suspensions with constant volume. (a) The dimensionless distance to the current front $R = r/r_\infty$ as a function of the dimensionless time $T = t/t_\infty$. (b) A dimensionless density of deposit $D_0 = \eta/\eta_0$ as a function of the dimensionless distance $R = r/r_\infty$. Symbols represent data of *Bonnecaze et al.* [1995] for experiments in geometries i–v (Figure 1), with initial and derived properties summarized in Table 1. Solid and dashed lines show the predicted relationships for currents in shallow and deep surroundings, respectively.

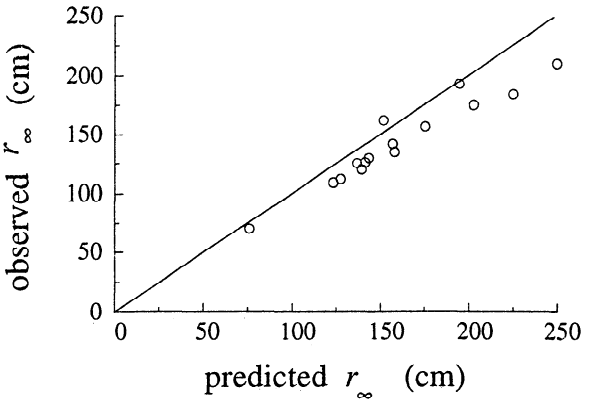

Figure 4. Comparison of predicted and observed runout distances for constant-volume, axisymmetric gravity currents, with properties summarized in Table 1. The solid line represents a one-to-one correspondence.

accommodate the effect of flow Reynolds number on the Froude number of a gravity current [*Riddell*, 1969] (also see the next section).

Flows With Constant Flux

Bonnecaze et al. [1995] also conducted representative experiments to measure the flow radius as a function of time and the particle deposit as a function of radius for an axisymmetric gravity current that resulted from the constant flux of a dense suspension. These experiments were conducted in one of the sector tanks used for the constant-volume flows (geometry i in Figure 1), modified to include a system for delivery of the suspension at constant flux. Further details are presented in the original study, but we note here that the delivery system could be adjusted so that the value of Fr of the introduced flow was near unity, and was designed to minimize entrainment of ambient fluid. The suspensions comprised 37- or 53-μm particles, g_o' was either 10 or 20 cm s^{-2}, and q' was either 75 or 130 cm^3 s^{-1} through a sector of 8° ($\Theta = 0.022$). The duration of each of the flows was about 70 s. The observations of *Bonnecaze et al.* [1995] are shown in Figure 5.

Several buoyancy-conserving gravity currents generated by the constant flux of saline solution were analyzed to determine suitable values of γ_f for the experimental setup of *Bonnecaze et al.* [1995]. This analysis can be motivated by noting that the solution of (2) for a buoyancy-conserving flow ($w_s = 0$), subject to constant Fr and the constant-flux constraint imposed by (22) yields the expression

$$r = \gamma_f (g_o' \dot{q} t^3)^{1/4}, \qquad (31)$$

where $\gamma_f = 0.78\, Fr^{1/2}$. Values of γ_f for three flows generated in the apparatus used by Bonnecaze et al. appear in Figure 6 as a function of a characteristic Reynolds number $uh/\nu = q/2\pi r\nu$. On the basis of this plot we selected a value of $\gamma_f = 0.85$ for further analysis of suspension-driven flows, but we note the weak dependence of this parameter on the dynamic state of the flow. Although this dependence is a source of error in our experiments, the magnitude of the error is small, as we shall see, and is, in any event, expected to be negligible in most geophysical applications.

With the estimate of $\gamma_f = 0.85$ we reconsider the data of Figure 5 in the dimensionless forms $R_f(T_f)$ and $D_f(R_f)$ for comparison with (28) and (30a). These comparisons appear in

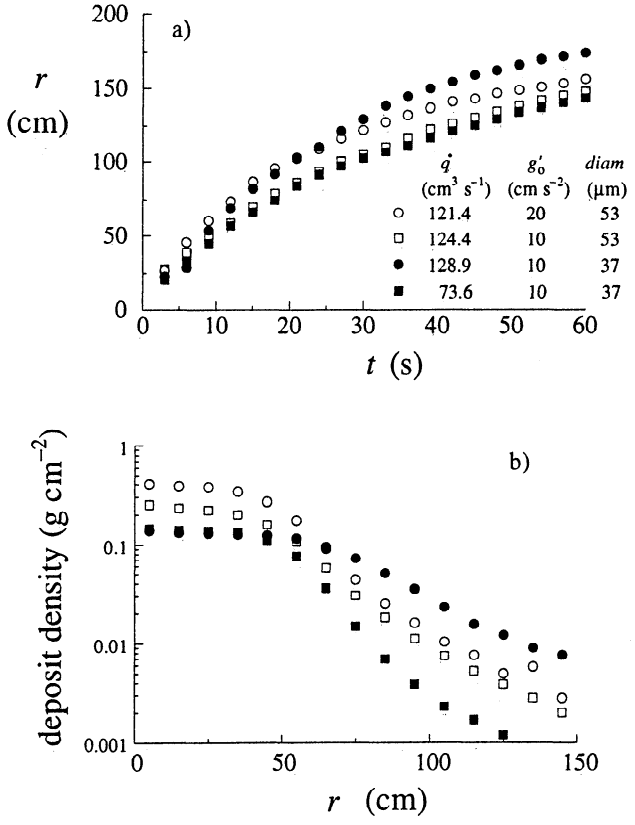

Figure 5. Data from the study of *Bonnecaze et al.* [1995] for gravity currents generated by the constant-flux release of dense suspensions. (a) Position of the current front as a function of time since release. (b) Mass deposited per area of bed as a function of radial distance from the point of release.

Figure 7. The data have been normalized by r_f and t_f given in (25) and (27) and by the observed η_o for each run. Again, we note that our analysis provides a good basis for the collapse of the available data. Also shown in Figure 7b are calculations for deposit geometry given by (19b) in terms of the approximate correlation $R \approx 2\, R_f$. This comparison reveals one of the key results of our analysis: delineation of the source conditions, constant volume versus constant flux, would appear to be practically impossible based on deposit geometry alone.

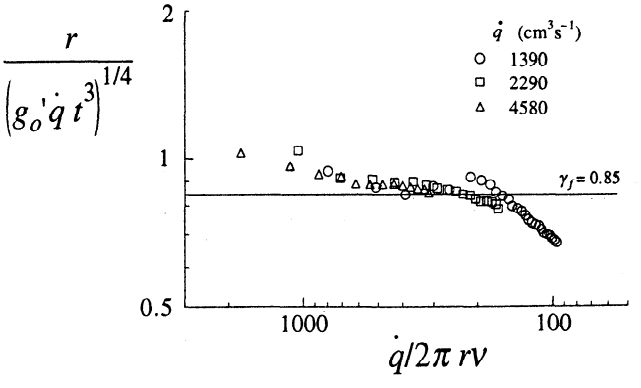

Figure 6. The dimensionless radial distance to the current front as a function of an effective Reynolds number $q/2\pi r\nu$ for constant-flux gravity currents in the sector-tanks used by *Bonnecaze et al.* [1995]. See text for further details.

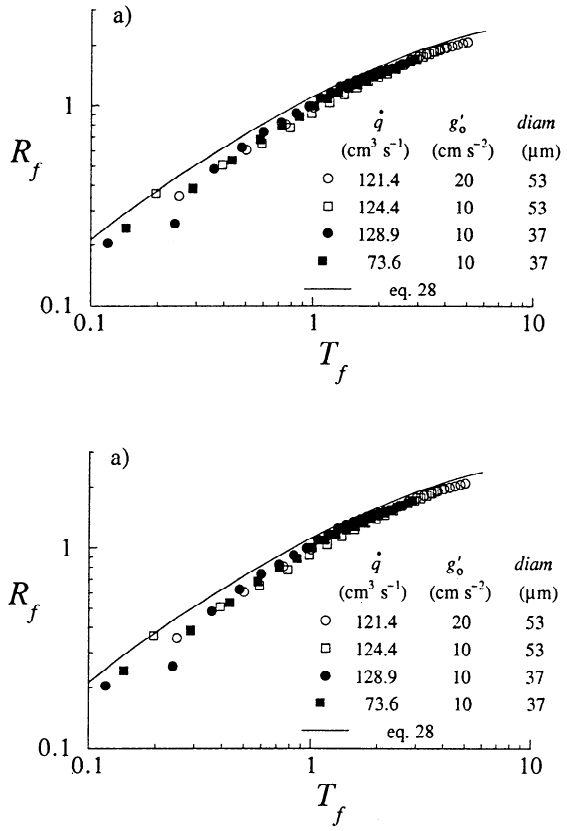

Figure 7. The runout and deposits of axisymmetrically spreading gravity currents generated by the constant-flux release of dense suspensions. (a) The dimensionless distance to the current front $R_f = r/r_f$ as a function of the dimensionless time $T_f = t/t_f$. (b) A dimensionless density of deposit $D_f = \eta/\eta_0$ as a function of the dimensionless distance $R = r/r_f$. Symbols represent data of *Bonnecaze et al.* [1995] for experiments with geometry i (Figure 1). The solid curve shows the predicted relationship. The dashed curve in Figure 7b shows the corresponding relationship for a constant volume-flow with $r_\infty \approx 2r_f$. See text for further details.

The Effect of Reversing Buoyancy on Runout

When the density of the ambient fluid exceeds that of the interstitial fluid of a suspension-driven gravity current, the deposit-forming flow is subject to a reversal of buoyancy. This possibility was introduced in our presentation of (2), and here we consider briefly the effects of this phenomenon on the runout length of a radially spreading flow.

When a reversal in buoyancy occurs, a gravity underflow will stall and then "lift off" from the bed at the radial distance r_{cr} where the particle concentration ϕ, progressively lost through deposition, equals ϕ_{cr} (see (2)). Beyond r_{cr} the density-driven underflow will terminate per se, and any material still in suspension will be carried aloft and dispersed over an area determined by residual momentum of the gravity current and background flow in the ambient fluid. This complication can be of considerable environmental importance. Buoyancy reversal and turbidity current "liftoff" may, for example, contribute to the formation and maintenance of some deep-sea nepheloid layers, or result in the generation of "hemiturbidites' which can in some instances be distinguished from turbidites [*Stow and Wetzel*, 1990]. More spectacularly, buoyancy reversal of a subacrial, pyroclastic ground surge (a suspension-driven gravity current which is analogous to turbidity currents in many respects) contributes to the formation of a co-ignimbrite cloud associated with some volcanic eruptions. Examples include the co-ignimbrite phenomena associated with the eruptions of Mount St Helens in 1980 and Mount Redoubt in 1991. These clouds may pose hazards to local air traffic, affect regional air quality, and influence global climatic conditions.

In the case of gravity flows with constant volume, we assess the effects of buoyancy reversal in broad terms by again rewriting (4) in terms of a spatial derivative but with nonzero ϕ_{cr}. The resulting equation has analytical solutions whose roots provide estimates of r_{cr}. These values are given in dimensionless terms as

$$R_{cr} = \left((1-\Phi_{cr})^{1/2} - \Phi_{cr}^{1/2} \arctan\{[(1-\Phi_{cr})/\Phi_{cr}]^{1/2}\}\right)^p \quad (32)$$

where the critical radial distance and concentration are normalized by r_∞ and ϕ_0, respectively, and the exponent p is 0.25 and 0.3 for deep and shallow surroundings, respectively.

In the case of a flow with constant flux, (24) yields the estimate

$$R_{fcr} = [-\ln(\Phi_{cr})]^{1/2}. \quad (33)$$

Beyond the straightforward predictions of (32) and (33), the descriptions for flow and suspension histories of a buoyancy-reversing gravity current require numerical analysis. As a first-order approach to the problem, however, we suggest that a gravity current can be evaluated, as described in our basic model, up to R_{cr} (or R_{fcr}). In the case of a constant-volume flow the assumption that a marine turbidity current runs out to near the full length given by $R = 1$ is, in any event, a reasonable one.

Consider, for example, a deep-sea turbidity current driven by a suspension of particles with the density of quartz and present in an initial concentration corresponding to $\phi_0 = 0.05$. If the flow is a constant-volume surge propagating into a basin of water that is 3% more dense than the interstitial water of the surge (corresponding, say, to the typical difference in density between surface and abyssal seawater and thus representing what one might expect as a maximal difference in fluid densities), then $\Phi_{cr} \approx 0.4$ and from (32) we find that $R_{cr} \approx 0.7$. That is, the flow would either stall or lift off and the underlying surge deposit thus be truncated at approximately 70% of the radial distance predicted by (7) and for which any difference in density of the interstitial and ambient fluids was ignored. At this reduced distance the deposit would have diminished to approximately 1/3 of the maximal thickness observed near the origin.

We point out that (32) and (33) represent minimum values for the distance to the current front at the instant of buoyancy reversal. Although we noted earlier that the constraint posed by (5) makes consideration of fluid entrainment unnecessary in general, assimilation of even small amounts of ambient fluid into a flow head [e.g., *Hallworth et al.*, 1993] will tend to bring the densities of interstitial and ambient fluids of that part of the gravity current into equilibrium, and thereby delay reversal.

Summary of the Analysis

We have developed a straightforward model that retains the essential physics of a deposit-forming gravity current which

undergoes radial collapse while propagating into a relatively flat basin. In our development of this model we assumed that the densities of interstitial and ambient fluids are equal, that entrainment of sediment and ambient fluid are negligible, and that the suspension of particles driving the gravity flow can be well characterized with a single settling velocity. Our model captures key aspects of experimental observations of flows driven by the release of either a constant volume or a constant flux of dense suspension.

Among the results of our analysis that should prove useful to geologists are the relationships between the radial extent or average thickness of a deposit and the initial properties of the deposit-forming flow generated by the release of a constant volume of dense suspension. These relationships are embodied in the expressions for r_∞ given in (7) and (13), and η_{av} given in (18) and (21) for deep and shallow surroundings, respectively. Analogous scalings for deposit geometry and the length and timescales pertaining to a flow driven by the constant-flux release of a dense suspension are given in (25), (27), and (30).

We have also discussed briefly the relevance of buoyancy reversal to the runout length of a deposit-forming gravity current. Predictions for the runout length of a turbidity current given by the basic models, however, are nevertheless probably accurate to within a factor of about 2, regardless of the potential for buoyancy reversal. We now extend the results of our analysis to the interpretation of some geologically significant deposits.

A Geological Application: Turbidites of the Hispaniola-Caicos Basin

Bennetts and Pilkey [1976] described the characteristics of three turbidites which are prominent features of the sedimentary fill of the Hispaniola-Caicos basin of the western Atlantic Ocean. The basin itself underlies approximately 4 km of water and is well defined by steep surrounding slopes. The relatively flat floor of the basin is characterized by regional slopes of 1/1000 or less and has an area of approximately 9500 km^2. In general, the deposits are oolitic- or bioclastic-rich calcarenites with $CaCO_3$ contents ranging from 44% to 81% by weight. Each deposit exhibits a roughly radial geometry (Figure 8), indicating that the spreading of the respective parent flows was roughly axisymmetric. Bennetts and Pilkey concluded from their analyses of constituent particles in each turbidite that each of the flows originated in the calcareous, shallow-water banks and shelves surrounding the basin but that each flow also accumulated a significant amount of fine material while descending the marginal slopes and into the basin. Each of the turbidity currents is speculated to have entered the basin by way of a narrowly channelized flow and then to have debouched and laid down its driving suspension to generate the turbidites now preserved. Relevant details of each deposit are summarized in Table 2.

We applied the scalings for deposit geometry derived from our model to infer the initial conditions of each of the sediment transporting flows as it entered the Hispaniola-Caicos basin. The following assumptions were made. Each of the turbidity currents was considered to have been a gravity surge of constant volume. The difference between interstitial and ambient fluid densities for each flow was negligible, and thus there was little or no potential for buoyancy reversal. Although the assumption that $\phi_{cr} \approx 0$ would follow from vigorous fluid entrainment during descent into the basin, we further assume that any effects due to entrainment became negligible once the current debouched upon the relatively flat floor of the basin. The characteristic grain size $\hat{a}$ for each suspension was taken to be the geometric mean of the minimum and maximum size, $a_{\min}$ and $a_{\max}$. We chose $a_{\min} = 4$ μm, which corresponds to the lower limit for silt-sized particles, and thus represents a natu-

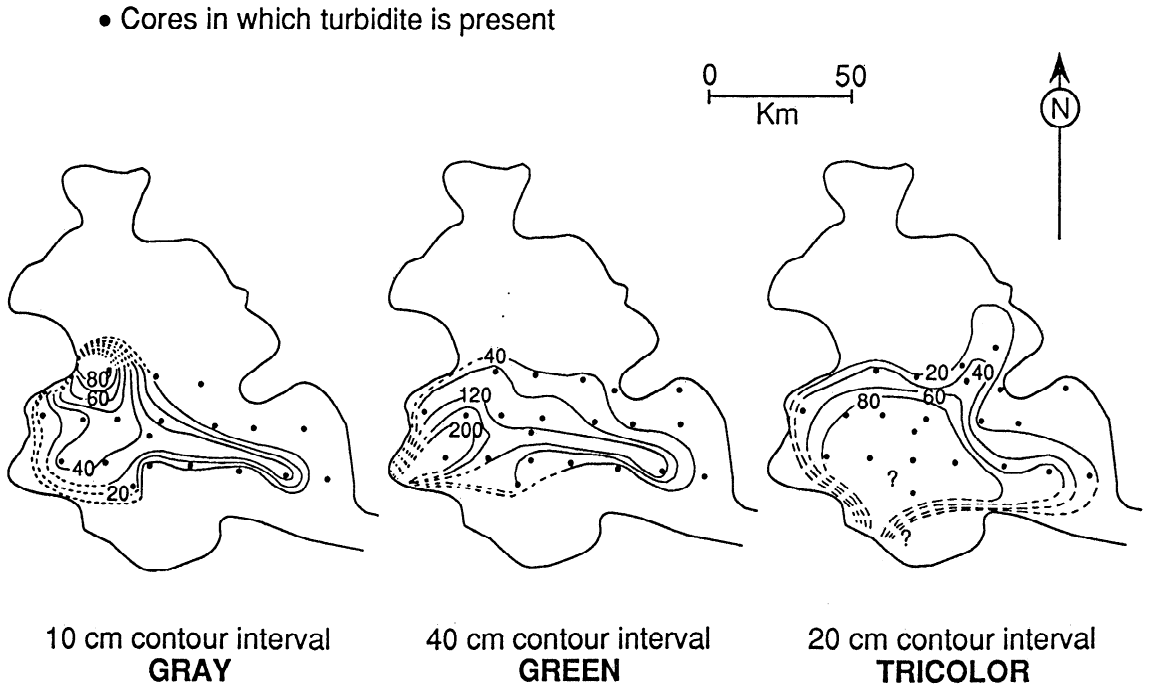

Figure 8. Isopach maps of turbidites of the Hispaniola-Caicos basin (redrawn from *Bennetts and Pilkey* [1976]).

Table 2. Reconstruction of Deposit-Forming Flows for Turbidites of the Hispaniola-Caicos Basin

Property	Definition	Turbidite Gray	Turbidite Green	Turbidite Tricolor
		Deposit Properties Reported by Bennetts and Pilkey [1976]		
q_s, km^3	sediment volume	0.9	3.1	2.6
η_{av}, m	average thickness	0.33	0.97	0.60
a_{max}, cm	maximal diameter	0.038	0.144	0.059
Probable rock type		oolitic biosparite	arenaceous lithosparudite	arenaceous biosparudite
		Assumed or Derived Properties of the Deposit		
a_m, cm	average diameter	0.004	0.008	0.005
w_s, cm s^{-1}	average fall speed	0.1	0.36	0.15
		Derived Properties of the Deposit-Forming Flow		
q_o', km^3	initial volume of flow	35	94	79
ϕ_o	initial sediment concentration	0.026	0.033	0.033
r_∞ km	runout length	59	64	74
t_∞ hours	runout timescale	5.5	3.5	5.3
$\hat{u}$, m s^{-1}	average speed	3.0	5.0	4.0

Turbidite colors refer to stratigraphic designation.

ral cutoff for turbidite muds and sands which are noncohesive. The maximum grain size a_{max} corresponds to the average largest clast size observed in each deposit by Bennetts and Pilkey [1976] and reported in Table 2. Nominal fall velocities for $\hat{a}$ were calculated using Stokes law for the settling of fine solitary particles and $\rho_p = 2700$ kg m^{-3}.

For a surge entering from a channel (treated as a point source) at the side of the basin, $\Theta^{-1} = 2$. For the sake of expedience we assume $\gamma_d = 1$. For a known volume of sediment with a solids fraction of 0.5 and a grain size distribution set by the deposit itself, there are no further degrees of freedom. Thus initial concentration can be calculated from a rearrangement of (18), for which $\phi_o = (\Theta\pi^4\phi_b^4\eta_{av}^4 g_p'/q_s' w_s^2)^{1/2}$. All other parameters that can be derived from our model then follow. The total flow volume q_o' is simply q_s/ϕ_o, and q_o, the idealized total volume for a flow spreading in all directions, is given by $\Theta^{-1}q_o'$. The runout distance r_∞ is calculated from (7), the characteristic runout time t_∞ is calculated from (11), and an estimate of a characteristic propagation speed of the front of the debouching current is $\hat{u} \approx r_\infty/t_\infty$. The results of this analysis are summarized in Table 2. A reconstruction of the Tricolor turbidity current and its deposit based on these results and (1), (10), and (19) appears in Figure 9.

In general, each of the turbidity currents considered here is inferred to have entered the Hispaniola-Caicos basin with a total volume of approximately 30–100 km^3 and a suspended solids concentration of about 0.03 (corresponding to a suspension density of about 80 kg m^{-3}). Each of the currents debouched into the basin with a characteristic speed of between 3 and 5 m s^{-1} and generated a deposit during a period of no

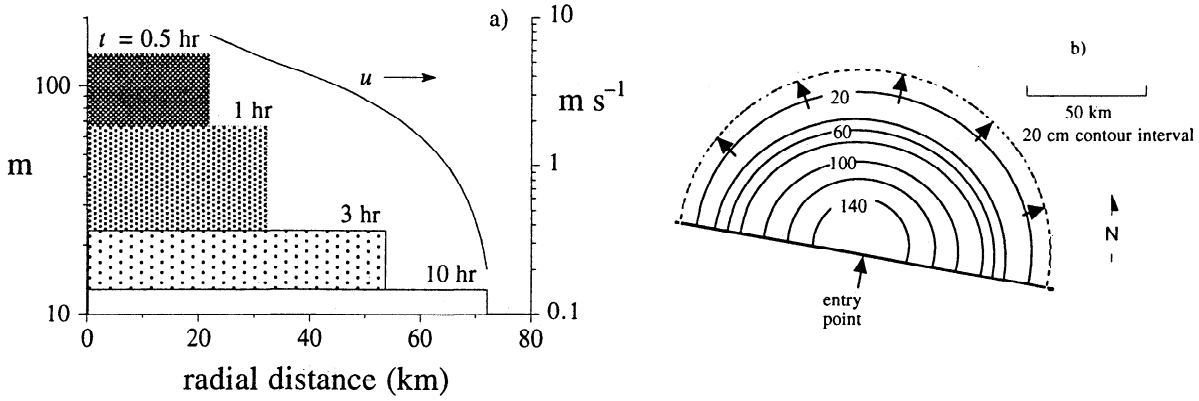

Figure 9. A reconstruction of the Tricolor turbidity current and deposit. (a) The thickness and propagation speed of the spreading, deposit-forming flow shown as functions of radial distance and time since entry into the Hispaniola-Caicos basin. The gradation in shading over time is meant to indicate the progressive loss of particles from the driving suspension. (b) Isopach map of the resulting model deposit (compare Figure 8). The arrows indicate axisymmetric flow of the deposit-forming event. The dashed line indicates the predicted runout length of 74 km, beyond which the deposit should essentially vanish. These reconstructions are based on calculations from our model for a constant-volume gravity current and the deposit properties summarized in Table 2.

more than about half a day. As the respective flows came to within 5 km of the ultimate runout distance each would have been about 10 m thick and advanced at a speed of less than 1 m s^{-1}. At this late stage, Coriolis effects may have become important, but we do not address those effects in this reconstruction. We note that even the coarsest material observed in the deposit by *Bennetts and Pilkey* [1976] would have been well mixed throughout the density current for most of the flow history, and so the settling law of (4) is consistent with our model flow conditions. Accordingly, the reconstructed deposit that resulted from the model Tricolor event reflects well the overall geometry of the actual turbidite. It diminishes from a maximal thickness of 160 cm expected near the origin to its "average" thickness of $2q_s/\pi\phi_b r_\infty^2$ = 60 cm at about 50 km radially distant from the point of entry into the basin. The deposit thins rapidly thereafter and vanishes at radial distances beyond r_∞ = 74 km.

In contrast, the Black Shell turbidite in the Hatteras basin has a sedimentary volume of about 100 km^3 [*Elmore et al.*, 1979]. A similar exercise in reconstruction of the flow which generated that approximately two-dimensional deposit [*Dade and Huppert*, 1994] suggests that upon entry into the Hatteras basin the Black Shell turbidity current had a similar concentration of suspended sediment but was approximately 10 times greater in initial volume than the individual turbidity currents of the Hispaniola-Caicos basin. As a result the Black Shell current travelled with a characteristic speed that was about twice that of, and lasted about four times as long as, the smaller events of the Hispaniola-Caicos basin. Relating the differences between the extent of deposits and magnitude and duration of the deposit-forming flows to the magnitude and probability of respective trigger events remains an outstanding geological problem (e.g., P. Beattie and W. B. Dade, Is scaling in turbidite deposition consistent with forcing by earthquakes, submitted to *Journal of Sedimentary Research*, 1995). Our models provide a basis for such inquiries, and it is our intention to continue to address these and other aspects of suspension-driven gravity currents.

Conclusions

We have developed an analytical model for the runout and deposition from a nonentraining gravity current driven by a dense suspension of fine particles and spreading axisymmetrically. In this model we incorporate simple flow geometries; source conditions of either constant volume or constant flux; a momentum equation that incorporates previously established Froude number conditions existing at the flow front; and a settling law for fine particles that exhibit a single, characteristic settling speed and that are in well-mixed suspension. The results of our study provide a useful basis for the analysis of a range of experimental observations and for the interpretation of geological deposits. We show, for example, that from limited information about a turbidite one can calculate the initial conditions and evolution of the parent flow as it debouched into a basin.

One important result of our study is that the overall geometries of well-sorted deposits generated by gravity currents with analogous source conditions corresponding to either constant volume or constant flux are virtually indistinguishable. Given this limitation, however, our model allows realistic reconstruction of a significant deposit-forming event based on the bulk properties of the resulting deposit alone.

Appendix A: Constraints on Sediment Erosion and Reworking

The ability of a gravity current to entrain sediment due to near-bed turbulence can be delineated in terms of the layer-averaged equations which describe the evolution of total volume, mean-flow momentum, and sediment volume for a flow section with constant radius. For a current which is not entraining ambient fluid these are, respectively,

$$\frac{\partial h}{\partial t}+\frac{1}{r}\frac{\partial}{\partial r}ruh=0, \tag{A1}$$

$$\frac{\partial}{\partial t}uh+\frac{1}{r}\frac{\partial}{\partial r}ru^2h+\frac{\partial}{\partial r}\frac{1}{2}g_p'\phi h^2=g_p'\phi\sin\beta-C_Du^2 \tag{A2}$$

$$\frac{\partial}{\partial t}\phi h+\frac{1}{r}\frac{\partial}{\partial r}ru\phi h=-w_s\phi+\overline{w'\phi'}, \tag{A3}$$

where all symbols are as defined in the main text and with the introduction of the areally averaged turbulent flux of sediment at the bed $\overline{w'\phi'}$ (= F_0h/q per (4)). Equations (A1) and (A3) reflect the notion that sediment volume is a small fraction of the total volume. Equation (A2) reflects the assumptions that vertical accelerations of the flow are negligible and that the essential momentum balance is one of inertial and buoyancy forces. The first two terms on the left-hand side of (A2), for example, are the total change in mean-flow momentum in time and space. The third term quantifies a hydrostatic pressure field that depends on the local density of the current. The first term on the right-hand side of (A2) reflects the downslope component of buoyancy which contributes to flow momentum, and the second term reflects momentum loss due to drag at the bed quantified by the coefficient C_D.

For our purposes here the body of a gravity current can be considered to be slowly varying (thus $\partial/\partial t \approx 0$) and the velocity field nearly uniform ($\partial u/\partial r \approx 0$). Under these conditions (A1)–(A3) can be combined to yield a relationship for the Froude number of the body of the flow given by

$$Fr_b^2\equiv\frac{u^2}{g_p'\phi h}=\frac{\sin\beta+\frac{1}{2}\left(w_s/u-\overline{w'\phi'}/u\phi\right)}{C_D}. \tag{A4}$$

Equation A4 is a modified Chezy equation [e.g., *Middleton*, 1993] which accommodates the effects of a gradient in hydrostatic pressure due to local sediment flux at the bed.

With (A1)–(A4) we additionally consider the equation which describes the evolution of the total turbulent kinetic energy kh in a section of the flow. *Parker et al.* [1986] demonstrated that this fourth equation was necessary for an accurate interpretation of a sediment-transporting gravity current. For a current that is not entraining fluid this equation is given by

$$\frac{\partial}{\partial t}kh+\frac{1}{r}\frac{\partial}{\partial r}khr=C_Du^3-\varepsilon h-\frac{1}{2}g_p'h\left(w_s\phi+\overline{w'\phi'}\right), \tag{A5}$$

[cf. *Parker et al.*, 1986]. The left-hand side of (A5) is the total change in the turbulent kinetic energy. The first term on the right-hand side of (A5) represents the rate of turbulence production due to mean-flow shear. In the second term, ε represents the layer-averaged rate of turbulence dissipation due to viscosity. These two terms typically constitute the bulk of a balance between sources and sinks of turbulent kinetic energy in a well-developed flow. If fine sediment in suspension is

present, however, the final term quantifies the work done by the flow at the expense of turbulent kinetic energy in maintaining the negatively buoyant suspension and in increasing the potential energy of the flow by way of sediment entrainment.

Following the reasoning of *Parker et al.* [1986], it is clear from (A5) that if the inequality

$$C_D u^3 > \frac{1}{2} g_p' h\left(w_s\phi + \overline{w'\phi'}\right) \tag{A6}$$

is not satisfied, then the turbulence in the body of the current will vanish. That is, the energetic demands on the dense suspension will exceed energy production, typically consumed primarily by viscosity in any event. As a result, maintenance of turbulence and particle suspension will occur only at the expense of mean-flow kinetic energy and thus the current itself will lose viability. Substitution of (A4) into (A6) and subsequent rearrangement of the resulting expression thus yield a constraint on the turbulent flux of sediment at the bed given by

$$\frac{\overline{w'\phi'}}{w_s\phi} < \frac{u \sin b}{w_s}. \tag{A7}$$

Equation (A7) corresponds to one form of the Knapp-Bagnold criterion for autosuspension, the condition under which a gravity current on a slope may accelerate dramatically due to a progressive increase in excess buoyancy by way of sediment entrainment at the bed [*Bagnold*, 1962; *Parker et al.*, 1986]. Here, however, we note an additional aspect of this constraint. In the case of a flow on a relatively shallow slope, that is if $w_s/u > \sin\beta$, not only is autosuspension energetically impossible to achieve, as has been noted by earlier workers, but also the ability of the flow to erode additional underlying sediment or even rework newly deposited material must be severely limited relative to the rate of fallout of suspended sediment $w_s\phi$. The high speed front of the current may indeed be erosive, but for our purposes we conclude that the term F_0 in (4) becomes negligible for most of the flow length if $w_s/u > \sin\beta$. Suspension-driven flows on beds of negligible slope, in other words, are necessarily and predominantly deposit-forming phenomena.

This conclusion is consistent with the notion that near-bed turbulence over most of the length of a deposit-forming gravity current is suppressed by a "moving bed." A moving bed, we speculate, consumes shear stress and reduces the competence of the flow to entrain sediment through the combined effects of buoyancy stratification and particle interactions. The thickness of such a layer must be limited by grain-flow interactions, and features in the resulting deposit, such as planar laminations and climbing ripples as are commonly seen in turbidites, should reflect its dynamics [e.g., *Allen*, 1984; *Lowe*, 1988; *Pickering et al.*, 1989]. As a part of this process, material newly arrived at the bed from the overlying suspension is thus undoubtedly subject to current reworking. Indeed it is difficult to imagine that the flow speeds of several meters per second considered here for deposit-forming turbidity currents in the Hispaniola-Caicos basin would not be capable of bed reworking to some extent (see, for example, *Garcia and Parker* [1993]). We suggest, however, that the downstream displacement of newly deposited material due to near-bed reworking from where we would have it come to rest following suspension fallout, is a higher-order aspect of the problem of turbidite deposition on low-angle slopes.

We provide here a possible explanation as to why a turbidity current debouching into a deep-sea basin must be predominantly depositional. The overall flow is driven by a density difference owing primarily to the overwhelming majority of mass of particles in suspension. This suspension is in energetic disequilibrium and, as we propose in the text, sediment mass must be lost from the main body of the suspension to create a deposit at a rate corresponding to the downward flux of sediment $w_s\phi$. Because the suspension is in disequilibrium, this can occur even in a gravity current propagating at what might otherwise be considered a strictly erosive speed.

Appendix B: Expression for $T = f(R)$ that Describes the Propagation of a Suspension-Driven Gravity Current into Shallow Surroundings

Here we present the explicit relationship

$$T = f(R) = -\frac{3}{10}\Bigg[\ln\left(1-R^{2/3}\right) + \sum_{n=1}^{4}\cos\left(2n\pi/5\right)\ln\left[1+R^{2/3}-2R^{1/3}\cos(n\pi/5)\right] - 2\sin\left(4n\pi/5\right)\left(\arctan\left\{\left[R^{1/3}-\cos\left(n\pi/5\right)\right]/\sin\left(n\pi/5\right)\right\} - \left(2n-5\right)\pi/10\right)\Bigg] \tag{B1}$$

between dimensionless time T and radial distance R introduced in (14).

Acknowledgements. We are grateful to R. Bonnecaze and J. Lister for stimulating discussions on axisymmetric gravity currents and to M. Hallworth and M. Elliott for considerable help in performing the experiments. R. Bonnecaze, G. Middleton, H. Pantin, S. Turner and two anonymous reviewers made helpful comments on earlier versions of the text. This research was supported by grants from the Natural Environmental Research Council (United Kingdom).

References

Abramowitz, M., and I. A. Stegun, *Handbook of Mathematical Functions*, 1046 pp., Dover, Mineola N.Y., 1965.

Allen, J. R. L., *Sedimentary Structures. Dev. in Sedimentol.*, vol 30(1-2), Elsevier, New York, 1984.

Bagnold, R. A., Auto-suspension of transported sediment, turbidity currents, *Proc. R. Soc. London A, 265*, 315-319, 1962.

Benjamin, T. B., Gravity currents and related phenomena, *J. Fluid Mech., 31*, 209–243, 1968.

Bennetts, K. R. W., and O. H. Pilkey, Characteristics of three turbidites, Hispaniola-Caicos basin, *Geol. Soc. Am. Bull., 87*, 1291–1300, 1976.

Bonnecaze, R. T., H. E. Huppert, and J. R. Lister, Particle-driven gravity currents, *J. Fluid Mech., 250*, 339–369, 1993.

Bonnecaze, R. T., M. A. Hallworth, H. E. Huppert, and J. R. Lister, Axisymmetric particle-driven gravity currents, *J. Fluid Mech., 294*, 93–121, 1995.

Dade, W. B., and H. E. Huppert, Predicting the geometry of deep-sea turbidites, *Geology, 22*, 645–648, 1994.

Dade, W. B., and H. E. Huppert, A box model for non-entraining, suspension-driven gravity currents on horizontal surfaces, *Sedimentology, 42*, 453–471 1995.

Dade, W. B., J. R. Lister, and H. E. Huppert, Fine-sediment deposition from gravity surges on uniform slopes, *J. Sediment. Res., A64*, 423–432, 1994.

Elmore, R. D., O. H. Pilkey, W. J. Cleary, and H. A. Curran, Black shell turbidite, Hatteras Abyssal Plain, western Atlantic Ocean, *Geol. Soc. Am. Bull., 90*, 1165–1176, 1979.

Garcia, M., and G. Parker, Experiments on the entrainment of sediment into suspension by a dense bottom current, *J. Geophys. Res., 98,* 4793–4807, 1993.

Hallworth, M. A., J. C. Phillips, H. E. Huppert, and R. S. J. Sparks, Entrainment in turbulent gravity currents, *Nature, 362,* 829–831, 1993.

Huppert, H. E., and J. E. Simpson, The slumping of gravity currents, *J. Fluid Mech., 99,* 785–799, 1980.

Lowe, D. R., Suspended-load fallout rate as an independent variable in the analysis of current structures, *Sedimentology, 35,* 765–776, 1988.

Middleton, G. V., Sediment deposition from turbidity currents, *Annu. Rev. Earth Planet. Sci., 21,* 89–114, 1993.

Parker, G., Y. Fukushima, and H. M. Pantin, Self-accelerating turbidity currents, *J. Fluid Mech., 171,* 145–181, 1986.

Pickering, K. T., R. N. Hiscott, and F. J. Hein, *Deep Marine Environments.* 416 pp., Unwin Hyman, Boston, Mass., 1989.

Riddell, J. F., A laboratory study of suspension-effect density currents, *Can. J. Earth Sci., 6,* 231–246, 1969.

Simpson, J. E., *Gravity Currents in the Environment and the Laboratory,* 244 pp., Ellis Horwood, Chichester, England, 1987.

Stow D. A. V., and A. Wetzel, Hemiturbite: a new type of deep-water sediment in *Proc. Ocean Drill, Program Sci. Results*, 116, 25-34, 1990.

W. B. Dade and H. E. Huppert, Institute of Theoretical Geophysics, Department of Earth Sciences and Department of Applied Mathematics and Theoretical Physics, University of Cambridge, Downing Street, Cambridge, England, CB2 3EQ. (e-mail: bdade@esc.cam.ac.uk)

(Received November 16, 1994; revised March 21, 1995; accepted June 19, 1995.)